https://doi.org/10.1016/j.compgeo.2020.103454

Dual porosity modelling of coal core flooding experiments with carbon dioxide

Hosking, L.J.[1*] and Thomas, H.R.[2]

[1]*Department of Civil and Environmental Engineering, Brunel University London, Kingston Lane, Uxbridge, Middlesex, UB8 3PH, UK*

[2]*Geoenvironmental Research Centre, School of Engineering, Cardiff University, Queen's Buildings, The Parade, Cardiff, CF24 3AA, UK*

Abstract

This paper presents the validation of a recently developed dual porosity numerical model and provides insights into coal core flooding experiments with N_2 and CO_2. Experimental data for anthracite coal from the South Wales Coalfield, UK, allows the coal-gas constitutive behaviour to be defined, leading to the validation of the model using gas flooding data for a 120 mm long and 70 mm diameter core. N_2 and CO_2 injection scenarios are considered with the coal initially saturated with CH_4. It is demonstrated that the model can simulate the physical and chemical phenomena involved in multicomponent gas flow and storage in coal. Further analysis shows that N_2 breakthrough in the effluent gas is controlled by dual porosity flow without significant influence of adsorption-desorption, whereas for CO_2 this influence is greater. Coal swelling caused by CO_2 is identified as the predominant factor, with the preferential displacement of adsorbed CH_4 being limited by the time scale of flow across the core relative to the CH_4 desorption kinetics. These insights are useful for future experiments concerning the influence of core size. The importance of using sorption data from intact coal rather than powdered coal is highlighted by comparing the numerical predictions and experimental measurements.

Keywords: Numerical modelling, Dual porosity, Coal, Core flooding, Carbon sequestration

[*]Corresponding author: Dr Lee J. Hosking (formerly of Cardiff University)
Department of Civil and Environmental Engineering, Brunel University London, Kingston Lane, Uxbridge, Middlesex, UB8 3PH, UK
Email: Lee.Hosking@brunel.ac.uk, Tel: +44 (0)1895 265376

1 Introduction

Considering the need to reduce both the electricity generation share of coal and CO_2 emissions from industry, there is a significant opportunity to use coal *in situ* for geological CO_2 sequestration. This is particularly relevant for emissions from industry, since industrialised regions are often close to remaining coal deposits and may be far away from other suitable reservoirs. Coal can store large amounts of CO_2 in the adsorbed phase even at relatively low pressures [1], reducing the risk of its migration by providing a secure trapping mechanism. There is also an opportunity to offset costs through CO_2-enhanced coalbed methane recovery (ECBM), albeit with the need to prevent greenhouse gas emissions associated with using the recovered gas. Despite the value that coal seam sequestration could bring to the growing portfolio of CO_2 utilisation and sequestration options, the issue remains that pilot trials have often struggled with CO_2 sorption-induced coal swelling, which leads to permeability loss and restricted injection rates [e.g. 1, 2]. Although well-characterised, our understanding of coal swelling at a basic level remains relatively poor and observations in the field are not consistent [1]. This indicates that the continued study of field conditions and coupled physical and chemical phenomena is needed, including but not limited to coal swelling. Towards this, the current work combines numerical modelling with laboratory data for the purposes of validation and providing insights into the observed behaviour which assist in the design of future experiments.

Reservoir-scale numerical modelling can improve our current understanding of the coal swelling and CO_2 injectivity behaviour observed in pilot trials, but is heavily reliant on the assigned simulation conditions and the accuracy of the underlying theory. Core flooding experiments provide excellent data towards these aims, since they measure the gas flow and storage behaviour under conditions that attempt to replicate those *in situ*. However, there are constraints on the sample size, sample integrity, and confining conditions that can be achieved compared to the *in situ* case. Validated numerical models therefore provide a means to overcome these constraints by translating the main physical and chemical behaviour to larger-scale applications.

Coal core flooding investigations have used samples taken from coalfields around the world with tests

performed under a range of conditions [3-8]. Tests on intact coal have used cores ranging from 77 mm in length [6] up to 334 mm in length [3], with diameters between 38 mm and 70 mm. The use of reconstituted coal, formed by a process of grinding and packing, has enabled core flooding experiments to be performed on cores up to 1 m in length [5] or on briquettes, such as the $300 \times 50 \times 50$ mm samples tested by Wang et al. [7]. Although reconstituted coal is easier and more economical to prepare in larger samples, the main drawback is that the naturally-occurring pore structure of coal [9] is highly disturbed. Nonetheless, the larger-scale tests do give more time for transient coal-gas interactions to take place, especially regarding competitive adsorption-desorption since the pore connectivity and available surface area are increased. Numerical analyses have sometimes accompanied the core flooding experiments [4, 6], providing more detailed analysis of the experimental observations related to gas flow rate and composition, sorption behaviour, coal deformation and permeability, and CH_4 displacement efficiency. The present work performs a similar analysis for the core flooding experiments by Hadi Mosleh et al. [8], but also provides a more detailed analysis of the evolution of multicomponent gas stored in the core. The aim is to provide new insights that can help determine the predominant coal-gas interactions that are responsible for the observed gas flow behaviour.

The numerical simulations presented in this work have been carried out using the reactive gas transport module of the coupled thermo-hydro-chemo-mechanical (THCM) model, COMPASS, developed by Thomas and co-workers [10-12]. This model was recently further developed for studying the coupled flow and storage behaviour of dual porosity systems involving multiphase, multicomponent chemicals and gas [13]. Hence, the work presented here pursues the validation of the enhanced model using benchmarks provided by data from a partner experimental programme [8, 14, 15]. Since this data refers specifically to multicomponent gas flow and interactions in coal, including CO_2, the validation process serves to demonstrate the suitability of the model for simulating CO_2 sequestration in coal. The numerical simulations also provide a means to analyse the physical and chemical behaviour responsible for the experimental observations. An overview of the theoretical formulation for dual porosity gas flow in coal and its numerical implementation is provided below. This is followed by an overview of the experimental programme and a description of how the data has been used as input for the numerical

simulations. Comparisons between the experimental and simulated core flooding data are presented alongside an assessment of the performance of the numerical model and an analysis of the coupled behaviour governing the results.

2 Dual porosity theoretical formulation and numerical solution

A summary of the dual porosity numerical model of multiphase, multicomponent chemical-gas transport, presented in full by Hosking et al. [13], is first provided in this section. This is followed by details of the particular constitutive relationships used in the present work to describe: (*i*) real gas mixture properties, (*ii*) kinetically controlled adsorption and desorption, (*iii*) the feedback of deformation on gas transport, and (*iv*) inter-porosity mass exchange. The results of the core flooding simulations are later presented in terms of the temporal evolutions of the effluent gas composition and the amount of gas stored in the coal core. The latter is calculated as the sum of the free gas stored in the fracture network and coal matrix pores and the adsorbed gas held at the coal surface. Details of the numerical solution procedure are also provided.

2.1 Governing flow equations

The full system of dual porosity governing equations for water transfer and the reactive transport of dissolved and gaseous chemical components is developed in its general form by Hosking et al. [13]. A dual continuum approach was adopted, whereby the fracture network and porous coal matrix are handled as distinct continua over the domain and the primary flow variables have fracture and matrix values at every analysis point. The equations are simplified for the purposes of the current work, since the core flooding experiments to be simulated were conducted on coal cores that had been air-dried for 24 hours [8]. Hence, the governing equations can be reduced to the transport of the i^{th} sorptive gas component in a mixture of n_g components in the dual continuum system, giving:

$$\frac{\partial\left(n_F c_F^i\right)}{\partial t} = -\nabla\cdot\left(c_F^i \mathbf{v}_F\right) + \nabla\cdot\left(D_{e,F}^i \nabla c_F^i\right) + \Gamma_x^i \tag{1}$$

$$\frac{\partial\left(n_M c_M^i\right)}{\partial t} + R_s^i = -\nabla\cdot\left(c_M^i \mathbf{v}_M\right) + \nabla\cdot\left(D_{e,M}^i \nabla c_M^i\right) - \Gamma_x^i \tag{2}$$

where the subscripts F and M denote the fracture network and coal matrix pore regions, respectively, n_F and n_M are the porosities, c_F^i and c_M^i are the concentrations of the gas components, t is time, R_s^i is the sink-source term for the accumulation or generation of the i^{th} gas component due to adsorption and desorption, which exists in equation (2) but not in equation (1) since the vast majority of surface area in coal exists in the porous matrix [16], $\mathbf{v}_F$ and $\mathbf{v}_M$ represent the advective velocities, $D_{e,F}^i$ and $D_{e,M}^i$ are the effective diffusion coefficients, and Γ_x^i is the sink-source term for inter-porosity mass exchange between the continua.

Application of Darcy's law gives:

$$\mathbf{v}_\beta = -\frac{k_\beta}{\mu_\beta}\nabla u_\beta \tag{3}$$

where the subscript β is the continuum identifier, i.e. $\beta = F$ for the fracture continuum and $\beta = M$ for the matrix continuum, k_β is the intrinsic permeability, μ_β is the absolute viscosity of the gas mixture, and u_β is the gas pressure, given by the real gas law:

$$u_\beta = Z_\beta RT \sum_{j=1}^{n_g} c_\beta^j \tag{4}$$

where Z_β is the compressibility factor, R is the universal gas constant, and T is the temperature.

The effective gas diffusion coefficients, $D_{e,F}^i$ and $D_{e,M}^i$, are given by:

$$D_{e,\beta}^i, = n_\beta \tau_\beta D_f^i \tag{5}$$

where τ_β is the tortuosity factor and D_f^i is the free fluid diffusion coefficient.

Definitions of the dual porosities n_F and n_M and dual permeabilities k_F and k_M are given in detail by

Hosking et al. [13]. In summary, the matrix continuum values are those for intact coal free from natural fractures (cleats) and any induced fractures, and the fracture continuum values are those of the fracture "zone" including open fractures, mineral infillings, and altered coal matrix surrounding the fractures. This is expressed mathematically as:

$$n_F = w_f n_F^L \tag{6}$$

$$n_M = n_T - n_F \tag{7}$$

$$k_F = w_f k_F^L \tag{8}$$

$$k_M = (1 - w_f) k_M^L \tag{9}$$

where the local fracture porosity, n_F^L, is the ratio of the volume of pores in the fracture zone to the total volume of the fracture zone, i.e. $n_F^L = V_F^P / V_F$. This becomes 1.0 for a clean fracture in the absence of any mineral infilling or altered coal matrix. The parameter w_f is the volumetric weighting factor, which is the ratio of the volume of the fracture zone to the total (bulk) volume, i.e. $w_f = V_F^T / V_T$.

The procedure that may be followed to determine equations (7) to (9) is described by Hosking et al. [13].

2.2 Gas mixture properties

Under the conditions of CO_2 sequestration in coal seams and therefore the associated core flooding experiments, the injection pressure and temperature can be near the critical point of CO_2 (7.38 MPa and 304.1 K). Hence, the key gas properties that depend on the pressure, temperature and composition can deviate from those predicted for an ideal gas and must be described using appropriate relationships. Following Hosking et al. [13], in this work the real gas compressibility is described using the Peng and Robinson equation of state with van der Waals mixing rules, and the real gas mixture viscosity is described using the semi-empirical model of Chung et al. [17].

2.3 Kinetically controlled adsorption and desorption

Gas sorption in coal occurs as a combination of adsorption on the surface and absorption into the bulk solid. Sorption may be further characterised as physisorption or chemisorption, the former being controlled by van der Waals interactions and the latter by the formation of chemical bonds between the sorbent and sorbate. The present work does not attempt to distinguish these various mechanisms and so sorption and adsorption are used interchangeably as the total of gas retained at the coal surface and in the bulk solid.

As mentioned in section 2.1, it can be seen from equations (1) and (2) that gas adsorption is considered in the matrix continuum but not in the fracture continuum, reflecting the fact that the vast majority of surface area in coal exists in the porous matrix [16]. Accordingly:

$$R_s^i = \left(1 - w_f\right)\rho_s \frac{\partial s_s^i}{\partial t} \tag{10}$$

where ρ_s is the coal density and s_s^i is the adsorbed amount of the i^{th} gas component.

Adsorption can be modelled as an equilibrium or kinetic process. Equilibrium adsorption may be included in the theoretical formulation by using a retardation factor in the first term on the left-hand side of equation (2). Formulations of this type do not explicitly consider the loss or gain of free gas molecules due to adsorption or desorption. Instead, adsorption is considered to delay the advance of the gas component considered. By contrast, the present work considered adsorption as a kinetic process described as a combination of two first-order rates, chosen ahead of a single first-order rate model to improve the accuracy in matching experimental data. This gives:

$$s_s^i = s_{s,1}^i + s_{s,2}^i \tag{11}$$

$$\frac{\partial s_{s,1}^i}{\partial t} = \tau_1^i\left(s_{s,\infty,1}^i - s_{s,1}^i\right) \tag{12}$$

$$\frac{\partial s_{s,2}^i}{\partial t} = \tau_2^i\left(s_{s,\infty,2}^i - s_{s,2}^i\right) \tag{13}$$

where the subscripts 1 and 2 are used to denote the terms relating to each of the adsorption rates, τ_1^i and τ_2^i, and $s_{s,\infty,1}^i$ and $s_{s,\infty,2}^i$ are the adsorbed amounts at equilibrium with the free gas phase.

Applying the method of separation of variables to equation (12) gives:

$$\int_{s_{s,1}^i|_n}^{s_{s,1}^i|_{n+1}} \frac{1}{s_{s,\infty,1}^i - s_{s,1}^i} ds_{s,1}^i = \int_{t|_n}^{t|_{n+1}} \tau_1^i dt \tag{14}$$

where n denotes the time step.

Performing the integrals in equation (14) over a time step Δt, assessing $s_{s,\infty,1}^i$ at the mid-interval, and rearranging gives:

$$s_{s,1}^i\big|_{n+1} = s_{s,\infty,1}^i\big|_{n+1/2}\left(1 - e^{-\tau_1^i \Delta t}\right) + s_{s,1}^i\big|_n e^{-\tau_1^i \Delta t} \tag{15}$$

Repeating the process of equations (14) and (15) for equation (13) then fully defines both terms on the right hand side of equation (11), thereby describing overall adsorption by the superposition of the two first-order rate models. Capacity factors, Q_1^i and Q_2^i, are introduced to partition the overall adsorption behaviour between the models, with the following constraints:

$$0 \leq Q_1^i \leq 1 \tag{16}$$

$$Q_2^i = 1 - Q_1^i \tag{17}$$

White et al. [18] discuss the development and validity of the theoretical and empirical models that can be used to calculate the adsorbed amounts at equilibrium, i.e. $s_{s,\infty,1}^i$ and $s_{s,\infty,2}^i$. The current work adopts the extended Langmuir isotherm, which in combination with equations (16) and (17) is expressed as:

$$s_{s,\infty,1}^i = \frac{Q_1^i s_L^i b_L^i \chi_M^i u_M}{1 + u_M \sum_{j=1}^{n_g} b_L^j} \tag{18}$$

$$s^i_{s,\infty,2} = \frac{Q^i_2 s^i_L b^i_L \chi^i_M u_M}{1 + u_M \sum_{j=1}^{n_g} b^j_L} \tag{19}$$

where s^i_L is the Langmuir capacity, b^i_L is the reciprocal of the Langmuir pressure, and χ^i_M is the mole fraction.

2.4 Deformation feedback

The governing equations presented in this work have been developed for flow in dual porosity deformable media. Coupled mechanical behaviour is not explicitly modelled; instead, the effect of deformation on gas flow is included by predicting the changes in porosity and permeability due to physical and chemical coal-gas interactions. The present work considers the sensitivity of permeability to changes in effective stress and the gas sorption-induced strain. The second of these is particularly significant for CO_2 and usually causes reductions in permeability of one or two orders of magnitude, although in extreme cases reductions of up to six orders of magnitude have been observed [19].

Many of the available closed-form coal permeability models were developed for application to field conditions based on the assumption of uniaxial strain [20, 21], making them unsuitable for the volumetric strain produced in core flooding tests under hydrostatic loading. To address this problem, Robertson and Christiansen [22] and Connell et al. [23] developed permeability models for hydrostatic confinement, with the latter of these being used in the present work. Variants of the model were given to deal with the different mechanical arrangements that may be encountered in core flooding experiments, including unjacketed, uniaxial (rigid radial), biaxial (rigid end), hydrostatic, and triaxial constraints.

For hydrostatic conditions, the cubic form of the model of Connell et al. is given by:

$$\frac{k_F}{k_{F,0}} = \left(\frac{n_F}{n_{F,0}}\right)^3 = \left\{1 - \frac{1}{n_{F,0}}\left[\frac{1}{K}(\tilde{u}_c - \tilde{u}_F) - (\beta - 1)\tilde{\varepsilon}^S_b\right]\right\}^3 \tag{20}$$

where the subscript 0 refers to the reference (initial) condition and the accent "~" is used to denote the

increment from this reference condition, K is the bulk modulus, u_c is the hydrostatic confining pressure, ε_b^S is the volumetric sorption strain, and β is a coefficient linking the volumetric sorption strain to the matrix sorption strain. The value of β can be determined by calibrating against experimental data [23].

The volumetric sorption strain, ε_b^S, in equation (20) is evaluated using a Langmuir strain isotherm. This approach has been used in all of the commonly used permeability models and is supported by comparisons with experimental data [e.g. 24, 25]. In multicomponent form and considering that sorption occurs only within the coal matrix (ref. section 2.3), the Langmuir strain isotherm yields:

$$\tilde{\varepsilon}_b^S = -\sum_{i=1}^{n_g}\left(\frac{\varepsilon_L^i b_L^i \chi_M^i u_M}{1+u_M\sum_{j=1}^{n_g} b_L^j} - \frac{\varepsilon_L^i b_L^i \chi_{M,0}^i u_{M,0}}{1+u_{M,0}\sum_{j=1}^{n_g} b_L^j}\right) \tag{21}$$

where ε_L^i is the Langmuir strain.

It is noted that equation (21) assumes the sorption strain is at equilibrium with the free gas phase. Although this is not consistent with the kinetically controlled gas sorption model given in section 2.3, it is considered a reasonable assumption for the purposes of the present work and development in this area is targeted in the future. Since coal matrix permeability, k_M, is usually around 8 orders of magnitude less than k_F [26], it is considered of secondary importance and therefore treated as a constant in the current work, giving $k_M = k_{M,0}$.

2.5 Inter-porosity mass exchange

The sink-source term controlling the rate of inter-porosity gas exchange, i.e. Γ_x^i in equations (1) and (2), is expanded in this section by assuming quasi-steady state distributions of gas pressure and concentration in the matrix blocks. In other words, there may be a pressure step at the fracture-matrix interface, but there are no pressure or concentration gradients between the fracture-matrix interface and the centre of a matrix block. Although this assumption is not strictly valid initially following a pressure step in the fracture , it allows Γ_x^i to be expressed as a linear function of the difference in fracture and matrix continuum pressures and concentrations [27]. The present work treats mass exchange as a diffusion

process, giving:

$$\Gamma_x^i = \sigma_D^i (c_F^i - c_M^i) \tag{22}$$

where σ_D^i is the first-order exchange rate due to diffusion, which can be expanded by considering the geometrical and material properties of the coal:

$$\sigma_D^i = \frac{\psi}{l^2} D_{e,\beta}^i \tag{23}$$

where ψ is a dimensionless factor relating to matrix block geometry, taken here as $2\pi^2$ [28], and l is the matrix block half-width.

2.6 Numerical solution

A numerical solution of the governing equations for dual porosity multicomponent gas transport is achieved by applying the finite element method with Galerkin weighted residuals for spatial discretisation, and an implicit mid-interval backward-difference scheme for temporal discretisation. A time splitting approach is used to couple the gas transport, inter-porosity mass exchange, and kinetically controlled sorption terms. Specifically, the sequential non-iterative approach (SNIA) is adopted, whereby conservative gas transport, mass exchange, and sorption are handled sequentially for each time step. In other words, each time step first involves solving the conservative transport equations assuming no mass exchange or sorption, and only once this system has converged are the gas concentrations updated in the mass exchange and chemical reaction modules. Such an approach has proven successful for sufficiently small time steps [11].

3 Overview of the experimental programme

The experimental programme conducted by Hadi Mosleh et al. [8, 14, 15] focused on characterising parameters and investigating processes that are important in the study of gas flow and storage in coal. Coal-gas interactions including sorption capacities and kinetics, and multicomponent flow behaviour were studied for He, N_2, CH_4 and CO_2. This was achieved using the two main analysis units of a bespoke

laboratory facility at Cardiff University; one for testing the sorption behaviour of size-distributed crushed coal samples and the other for testing the flow and deformation behaviour of intact coal cores. A schematic diagram of the facility is provided in Figure 1. Full details of the experimental setup, development and application are provided by Hadi Mosleh et al., although a summary is provided here for completeness.

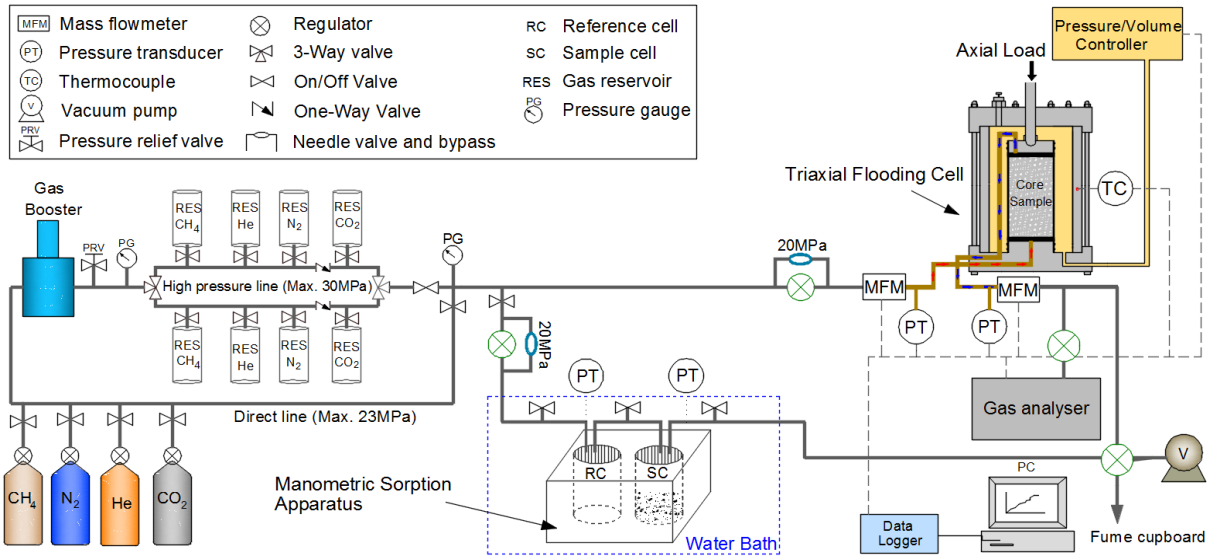

Figure 1 A schematic diagram of the experimental facility used to determine coal sorption capacity and kinetics and for core flooding experiments with He, N_2, CH_4 and CO_2.

3.1 Description of the apparatus

Measurements of the gas adsorption-desorption behaviour of coal are made using a manometric unit consisting of a reference cell and a sample cell connected via a needle valve. Pressure transducers monitor the gas pressure in each of the cells, which are contained within a water bath for temperature control. The design pressure and temperature are 20 MPa and 338 K, respectively. The main part of the flow measurement unit is a triaxial cell for cores of up to 0.1 m in diameter and 0.2 m in length. Prior to testing, a core is wrapped in a rubber sleeve, to which the confining pressure is applied using silicone oil and a pressure-volume controller. Uniform flow across the upstream and downstream faces of the core is promoted using diffusion plates. An axial load of up to 50 kN may be applied through a loading ram, although for the coal core flooding experiments considered in this work no axial load was applied, leading to conditions of hydrostatic confining pressure (making equation (20) applicable). The design

gas injection pressure is 20 MPa and there are flow meters and pressure transducers upstream and downstream of the core. Heating elements are used to regulate the temperature from ambient temperature up to 338 K.

3.2 Materials and methods

Information on the coal characteristics and experimental methods used by Hadi Mosleh et al. [8, 14, 15] is important to ensure that the material parameters and conditions used in the numerical simulations replicate the experiments as far as possible. The anthracite coal samples used were provided by Unity Mine, Wales, UK, having been taken from the Six Feet seam at a depth of 550 m. The physical and chemical properties of the coal are provided in Table 1.

Table 1 Characteristics of the coal used by Hadi Mosleh et al. [8].

Moisture content (%)	1.2	Carbon (%)	86.4
Ash content (%)	4.9	Sulphur (%)	0.8
Volatile matter (%)	9.7	Bulk density (kg m^{-3})	1398
Fixed carbon (%)	84.4	Total porosity (-)	0.05

Adsorption-desorption measurements were performed using 50 g samples of air-dry powdered coal, sieved to ensure 0.5 to 1 mm grain sizes. Each test began with a vacuum pump being used to evacuate the pipes, valves, and reference and sample cells to prevent contamination. The void volume with and without the sample was determined using He pycnometry. Following this, the system was vacuumed at −100 kPa for 24 hours to remove residual gas and moisture from the sample. Adsorption-desorption behaviour was measured at 298 K by varying the gas pressure in a stepwise manner at 0.5, 1.0, 2.0, 3.0, 4.2, 5.5 and 7.0 MPa. It is noted that the accuracy of applying parameters obtained using powdered coal to model the intact coal cores is part of the analysis of simulation results presented in this work.

Core flooding tests were performed on coal cores 120 mm long and 70 mm in diameter and began with the application of a vacuum for 24 hours followed by saturation with the required gas. Two coal cores were used; core A and core B. Permeability measurements using core A were performed for the steady-

state flow of He, N_2, CH_4 and CO_2 at injection pressures of up to 5.5 MPa and confining pressures of up to 6 MPa. Multicomponent gas flow and storage tests using core B were performed considering CH_4 displacement first by N_2 and then by CO_2. These tests involved saturating the core with CH_4 at 5 MPa at 6 MPa confining pressure with the downstream valve closed, followed by the injection of N_2 or CO_2 also at 5 MPa with the downstream valve opened to initiate flow. A temperature of 298 K was maintained in all flooding tests with atmospheric pressure at the downstream face. The order of experiments performed on both cores is shown in Figure 2 and is explained in full by Hadi Mosleh et al. [8, 15]. Highlighted boxes represent the tests considered as benchmarks in the current work; the two numerical simulations presented in the following section are for the displacement of CH_4 by N_2 and CO_2, respectively, using core B.

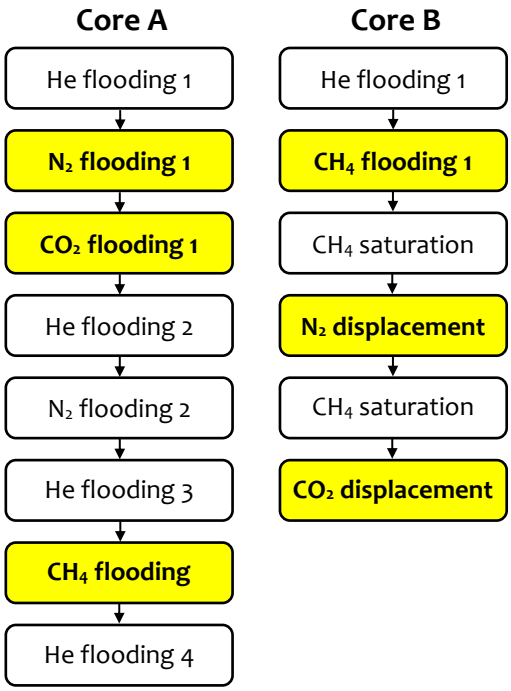

Figure 2 Order of the experiments performed using cores A and B with highlighted cells indicating those used as benchmarks in the current work.

4 Adsorption-desorption and permeability behaviour

Before the numerical model can be applied to simulate the multicomponent core flooding experiments, the coal properties considered in the theoretical formulation must be defined. It is particularly important to have a good understanding of the adsorption-desorption and permeability behaviour of the coal in

order to define the models presented in sections 2.3 and 2.4. Accordingly, Table 2 provides the sorption parameters used for the numerical simulations based on the averages of the relevant experimental data presented by Hadi Mosleh [29]. Figure 3 shows the resulting sorption isotherms for N_2, CH_4 and CO_2.

The sorption kinetics measurements and fitted model predictions can be seen in Figure 4, expressed in terms of the residual (unoccupied) sorption capacity, s_r^i, given by:

$$s_r^i = \frac{s_{s,t}^i - s_{s,\infty}^i}{s_{s,0}^i - s_{s,\infty}^i} \tag{24}$$

Table 2 Parameters fitting the adsorption-desorption data of Hadi Mosleh et al. [29].

Gas	Langmuir capacity s_L^i (mol kg^{-1})	Langmuir constant, b_L^i (Pa^{-1})	Sorption rate τ_1^i (s^{-1})	Sorption rate τ_2^i (s^{-1})	Capacity factor Q_1^i
N_2	0.67	5.8×10^{-7}	5.0×10^{-4}	4.1×10^{-5}	0.35
CH_4	1.07	1.5×10^{-6}	3.0×10^{-4}	3.6×10^{-5}	0.20
CO_2	1.32	0.2×10^{-6}	7.0×10^{-4}	5.5×10^{-5}	0.85

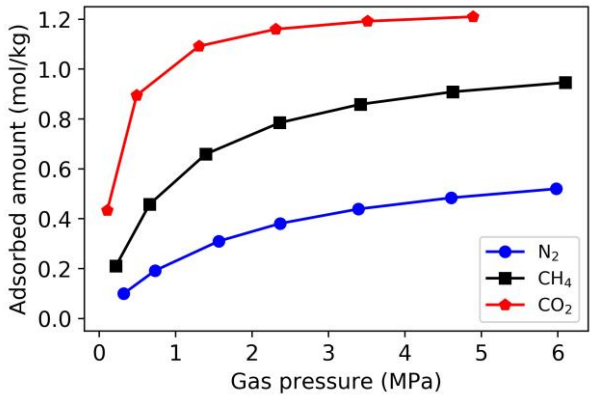

Figure 3 Sorption isotherms for N_2, CH_4 and CO_2 [29].

For each gas, τ_1^i refers to the initially rapid stage of adsorption and τ_2^i refers to the more gradual stage that follows. As per equations (16) to (19), the capacity factors Q_1^i and Q_2^i are used to partition the contribution of each of these stages to the overall kinetics. It can be seen that CO_2 adsorption is dominated by the rapid first stage, giving $Q_1^{CO_2} = 0.85$. For N_2 and CH_4, the kinetics depend more on the slower second stage, giving $Q_1^{N_2} = 0.35$ and $Q_1^{CH_4} = 0.2$. This behaviour may be controlled by the

contributions of mesopores and micropores to the sorption capacity, as well as the pore connectivity. It is reasonable to expect that the distributions of mesopores (2 to 50 nm) and micropores (< 2 nm) would have been largely unaffected in the preparation of the 0.5 to 1 mm grain size samples [30]. It could then be inferred that the rapid first stage of adsorption occurs in the more open mesopores, with the subsequent slower stage occurring in the less accessible micropores. This would go some way to explaining the observed behaviour, since it has been postulated that N_2 and CH_4 adsorb mainly in the micropores, whereas CO_2 adsorbs both in micropores and in multiple layers in mesopores [31]. Furthermore, the pore connectivity of the coal may have been highly constricted by ultra-micropores with a width less than 0.6 nm. This would be relevant since Cui et al. [30] found that CO_2 can access pores with a smaller half-width (0.289 nm) compared to N_2 (0.305 nm) and CH_4 (0.31 nm).

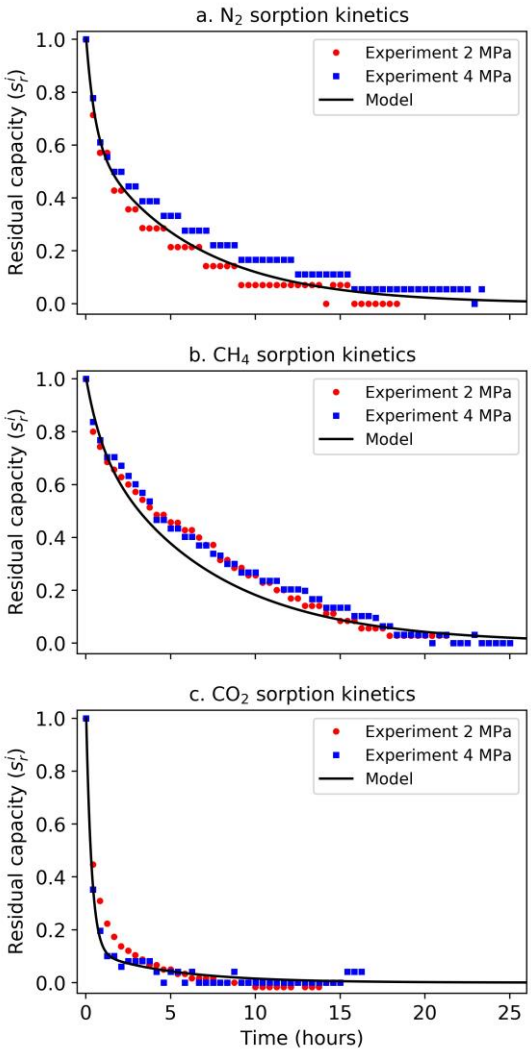

Figure 4 Comparisons between the experimental sorption kinetics measurements and the fitted predictions of the combined two first-order rate model.

Figure 5 compares the permeability data obtained in the experiments [15] and the calibrated (fitted) predictions made by the model of Connell et al. [23]. Gas pressures are displayed as the mean of the injection (upstream) pressure and downstream pressure and the corresponding material parameters are provided in Table 3. The value for Young's modulus, E, is based on measurements by Zagorščak and Thomas [32] on coal collected from the South Wales Coalfield, UK. A combination of literature review and fitting of the experimental results was used to determine Poisson's ratio, υ [22, 25], the initial fracture porosity, $n_{F,0}$, and the Langmuir strains, ε_L^i [22, 23]. The selected value of $n_{F,0}$ is similar in magnitude to the range of 0.002 to 0.004 suggested for coal from the San Juan basin, USA [24]. In each case, the initial fracture permeability, $k_{F,0}$, was taken as the value determined in the laboratory for the middle pressure step. The coefficient $\beta = 1.3$, which is similar to that used by Connell et al. ($\beta = 1.4$).

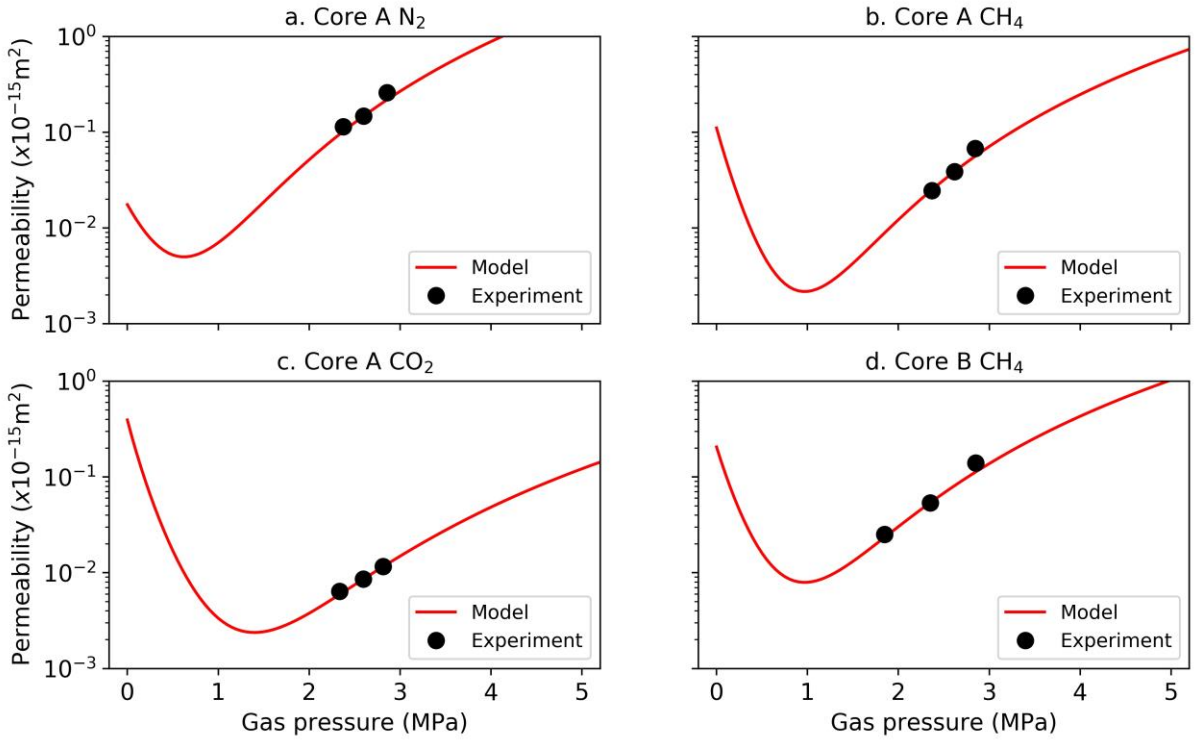

Figure 5 Comparisons between the experimental permeability measurements and the fitted predictions made by the permeability model of Connell et al. [23].

It can be seen that the material parameters described above give a good agreement between the experimental measurements and the predicted permeability curves. Whilst only a narrow range of effective stress conditions is considered, the permeability model has been validated [23] and applied [4] against other experimental core flooding data covering a wider range of effective stress and so may be

relied upon.

The trends shown in Figure 5 follow those expected considering the aforementioned sensitivity of coal permeability to effective stress and sorption-induced strain. Permeability rebound at low pressure is regulated by desorption-induced coal shrinkage and is therefore strongest for CO_2 and weakest for N_2. The significant rebound for both CO_2 and CH_4 is attributed to their particularly low Langmuir pressures ($1/b_L^i$) of 0.5 MPa and 0.68 MPa, respectively. Since these are the pressures at which half of the adsorption capacity is reached, a considerable amount of the sorption strain behaviour (coal swelling or shrinking) is contained within the low-pressure region. This contributes to the behaviour observed as the gas pressure increases from the initial value, whereby the permeability increases in all cases as a result of the effective stress dependence being dominant over the sorption strain dependence.

Table 3 Parameters fitting the permeability data of Hadi Mosleh et al. [15].

Parameter	**Value or relationship**
Young's modulus, E (GPa)	1.0
Poisson's ratio, υ (-)	0.3
Bulk modulus, K (Pa)	$K = E/3(1-2\upsilon)$
Initial porosity, $n_{F,0}$ (-)	0.001
Initial permeability, $K_{F,0}$	Value at middle pressure step [15]
β coefficient (-)	1.3
Langmuir strains, ε_L^i (-)	
N_2	0.008
CH_4	0.01
CO_2	0.018

5 Multicomponent core flooding simulations

As indicated by Figure 2, the two core flooding simulations presented in this work correspond to the displacement of CH_4 from core B using N_2 and CO_2. Figure 6 shows the 2-dimensional simulation domain formed by taking advantage of the axisymmetric nature of the coal core. The domain was spatially discretised using 100 equally sized axisymmetric 4-noded quadrilateral elements. Initial and boundary conditions were prescribed according to the experimental method described in section 3.2. In

summary, the domain was isothermal at 298 K with a constant confining pressure of 6 MPa, and initially contained gas at 5 MPa at equilibrium with the adsorbed phase. The initial gas composition was 99% CH_4 with 1% N_2 or CO_2 to prevent negative concentrations due to numerical oscillations. Gas injection was prescribed using a fixed pressure of 5 MPa for the fracture continuum at the upstream boundary and the downstream boundary was restrained at atmospheric pressure. A simulation period of 1 hour was considered.

Many of the material properties of the coal-gas system were assigned based on the adsorption-desorption and permeability behaviour discussed in the previous section. Hence, the values given in Table 2 and Table 3 were used with the exception of the initial fracture permeability, $k_{F,0}$, which was instead determined by extrapolating Figure 5d towards a CH_4 pressure of 5 MPa. This provided a good estimate for $k_{F,0}$ since Figure 5d presents data obtained for core B for the flow of CH_4 at a confining pressure of 6 MPa, i.e. the same gas (at the initial condition) and confining pressure that were used in the multicomponent core flooding experiments. A value for $k_{F,0}$ in the region of 1.5×10^{-15} was indicated with the final value of 2.0×10^{-15} m^2 being found to give the best match to the experimental data. Following the discussion in section 2.4, $k_{M,0}$ was assigned a value of 2.0×10^{-23} m^2.

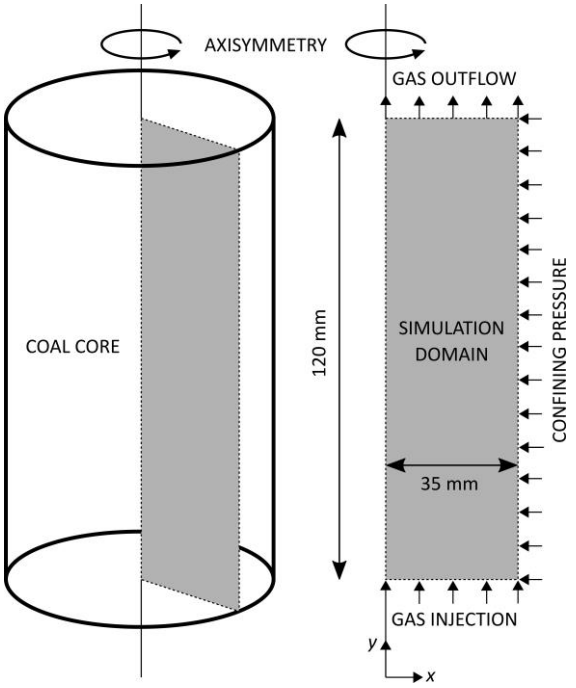

Figure 6 Geometry of the coal core and the 2-dimensional axisymmetric simulation domain used for the numerical simulations.

In the absence of supporting data, the volumetric weighting factor, w_f, was used as a fitting parameter leading to the chosen value of 0.002. This indicates that the fracture zone, which includes the volume occupied by open fractures, mineral infillings, and the altered coal matrix [13], occupies 0.2% of the bulk volume. Substituting $n_F = 0.001$, as established in section 4, into equation (6) implies a local fracture porosity, n_F^L, of 0.5. Using equation (7) with $n_T = 0.05$ (Table 1) gave $n_M = 0.049$. Finally, the free fluid diffusion coefficients, D_f^i, were taken from Cussler [33]. These parameters are reported in Table 4.

Table 4 Parameters in addition to those provided in Table 1, Table 2 and Table 3 required for the numerical simulations of the multicomponent core flooding experiments.

Parameter	**Value or relationship**
Volumetric weighting factor, w_f (-)	0.002
Local fracture porosity, n_F^L (-)	0.5
Matrix porosity, n_M (Pa)	0.049
Initial fracture permeability, $K_{F,0}$ (m^2)	2.0×10^{-15}
Matrix permeability, K_M (m^2)	2.0×10^{-23}
Free fluid diffusion coefficient, D_f^i (m^2s^{-1})	
N_2	2.0×10^{-5}
CH_4	2.2×10^{-5}
CO_2	1.1×10^{-5}

5.1 Simulation results and analysis

Figure 7 shows the evolution of the effluent gas composition observed in the multicomponent core flooding experiments and predicted by the numerical simulations. It can be seen that there is a good agreement between the data sets. The curves are characterised by a sharper initial breakthrough followed by a more gradual secondary breakthrough; the former being governed by the displacement of free CH_4 in the fractures and the latter by the displacement of free and adsorbed CH_4 stored in the coal matrix along with the associated permeability changes. A close agreement can be seen in Figure 7a for N_2, albeit that the breakthrough is slightly delayed compared with the experiment, whereas for CO_2 in Figure 7b the simulation predicted an earlier yet more gradual initial breakthrough, as well as a slightly more sustained increase in CO_2 composition in the later stages. The N_2 core flooding simulation indicates that

the rate of bulk flow may be slightly underpredicted by the model. By considering that CO_2 breakthrough occurred earlier than in the experiment, it could then be inferred that the influence of CO_2 adsorption-induced coal swelling is also underpredicted in the CO_2 simulation. A sensitivity analysis is beyond the scope of the present work but will be undertaken in the future to investigate these observations in greater detail. Nonetheless, overall there is a good agreement between the trends of the experimental observations and numerical predictions and the validation exercise is considered a success. The remainder of this section therefore explores the results in terms of the salient physical and chemical behaviour involved.

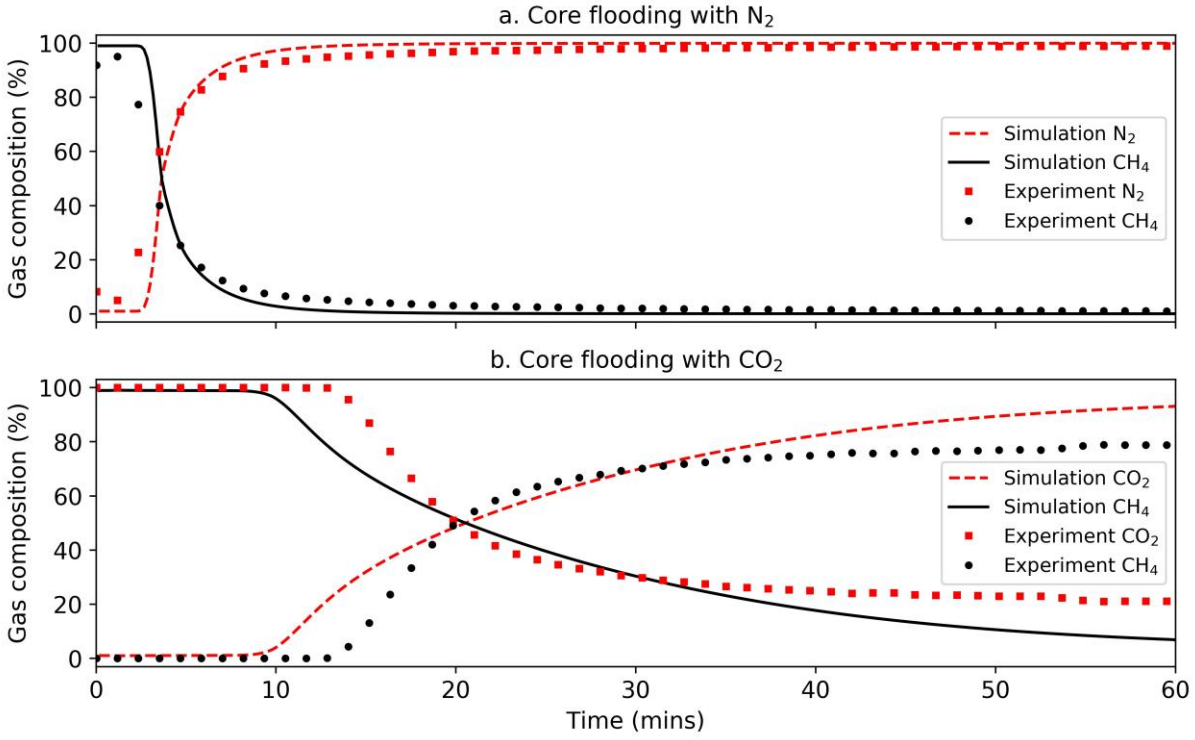

Figure 7 Effluent gas compositions observed in (a) the N_2 and (b) the CO_2 core flooding experiments compared with the predictions of the numerical model.

Initial breakthrough (in the simulations) occurred at 3 minutes for N_2 but took 10 minutes for CO_2 due to the loss of fracture permeability associated with sorption-induced coal swelling, which varies in magnitude with ε_L^i as CO_2 > CH_4 > N_2. The injection of CO_2 led to a greater residual fraction of CH_4 in the effluent gas than for the injection of N_2. To analyse this behaviour, it is important to reiterate the major species dependent coal-gas interactions, namely that: (*i*) coal has a preference to adsorb CO_2 over N_2 and CH_4 (Figure 3), and adsorption of CO_2 occurs more rapidly (Figure 4), and (*ii*) as above, sorption-

induced swelling is greatest for CO_2. In relation to point (*i*), the lower tendency of N_2 to displace adsorbed CH_4 implies that the displacement was less efficient than that by CO_2. In relation to point (*ii*), the larger CO_2 sorption-induced strains restricted the flow rate and limited the contribution of CO_2 to the effluent gas. In contrast, the higher flow rate maintained for N_2 meant that more of the injected gas arrived at the downstream boundary, increasing its contribution to the effluent gas relative to CH_4.

The nature of gas flow and deformation feedback is examined in greater detail by considering the spatial distributions of gas composition and coal permeability in the fracture continuum, as shown in Figure 8. Simulation results after 120 seconds are presented since at this early time the breakthrough of N_2 or CO_2 has not occurred, making it easier to distinguish the influence of the upstream and downstream boundary conditions. The trend of CH_4 displacement is similar, with N_2 having advanced further than CO_2, which is consistent with Figure 7. As expected, there are major differences between the distributions of fracture permeability, which increases by almost 1.5 times $k_{F,0}$ for N_2 and decreases by over 100 times $k_{F,0}$ for CO_2 injection. This behaviour is attributed to sorption-induced coal shrinking (for N_2) and swelling (for CO_2), which influences the fracture porosity and permeability according to equation (20). In both cases, there is significant permeability loss towards the downstream boundary as a result of the increase in effective stress as the initial CH_4 pressure of 5 MPa is reduced by the 0.1 MPa boundary condition. This effect is somewhat mitigated in Figure 8a by the more rapid advance of N_2.

To determine the predominance of adsorption-desorption behaviour in the experiments, it is useful to consider Figure 9 showing the temporal evolution of the amount of gas stored (Figure 9a and b) and the percentage present as free gas rather than adsorbed gas (Figure 9c and d). It can be seen that for both N_2 and CO_2 injection around 40% of the initial CH_4 remained in the core at the end of the simulation period. Despite this similarity, there are significant differences in the amounts of N_2 (0.24 mol) and CO_2 (0.63 mol) stored, with the free phase contributing 16% and 6%, respectively. In addition, the overall trends of CH_4 displacement are different for N_2 and CO_2 injection, with the rate of displacement by N_2 being initially faster than by CO_2 (up to 20 mins) before becoming more gradual later in the simulation. Comparison of the % free curves in Figure 9c shows that the pre-20 mins stage was characterised by

the almost total displacement of free phase CH_4 by N_2, after which CH_4 storage approached 99.9% in the adsorbed phase. A similar analysis of Figure 9d shows that a greater amount of free phase CH_4 was present throughout the simulation, which can be attributed to both the slower displacement of CH_4 initially stored in the pores (due to the lower flow rate) and the stronger displacement of adsorbed CH_4 by CO_2. These findings are consistent with those of Hadi Mosleh et al. [8] with additional insights provided here through the analysis of the free gas phase.

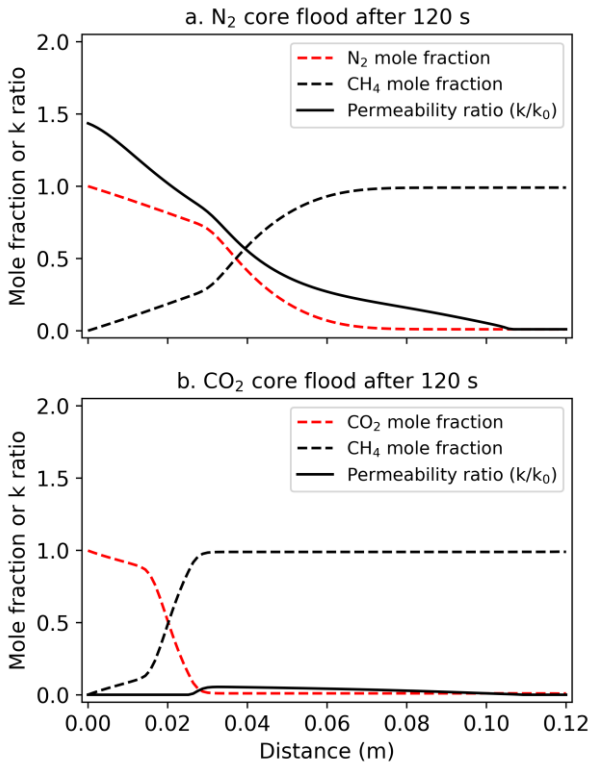

Figure 8 Spatial distributions of gas mole fraction and permeability ratio in the fracture continuum after 120 seconds in the numerical simulations of (a) the N_2 and (b) the CO_2 core flooding experiments.

It is apparent that the breakthrough of N_2 in Figure 7a was predominantly governed by bulk gas flow behaviour without significant influence by adsorption-desorption. Adsorbed CH_4 was displaced slowly even when pure N_2 had become established as the flowing gas, indicating that the residual CH_4 present in the effluent between 3 mins (following initial breakthrough) and 20 mins was due to mass exchange of free phase CH_4 from the matrix pores. Adsorption-desorption behaviour was more significant for the breakthrough of CO_2 shown in Figure 7b. Most notably this refers to adsorption-induced coal swelling, since the role of preferential CH_4 desorption was limited by the desorption kinetics being slow relative

to the time scale of flow across the 120 mm long core. As a result, a significant amount of CH_4 remained adsorbed at the end of the simulations, which can be inferred from Figure 9.

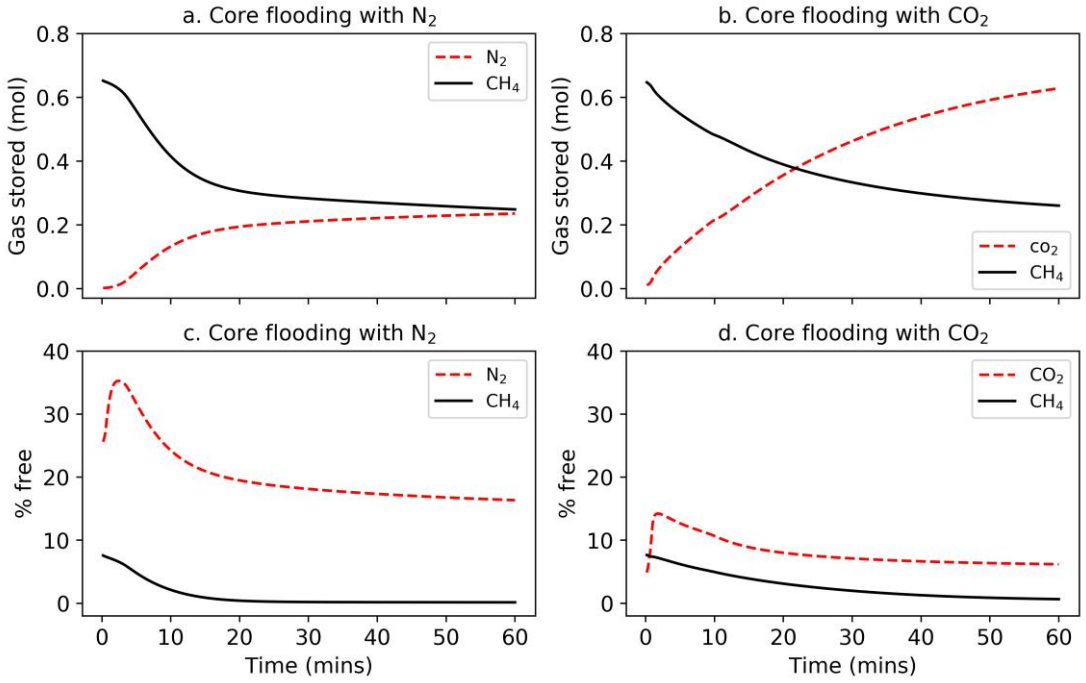

Figure 9 Evolution of the amount of gas stored in the coal core and the percentage present as free gas, as predicted by the numerical model.

An important observation is that the amount of CH_4 displaced in the numerical simulation follows a similar trend as the experiments but with a different magnitude. Specifically, the model predicted the displacement of 0.4 mol for N_2 injection and 0.39 mol for CO_2 injection after 1 hour, compared to 0.16 mol (60% less) and 0.12 mol (69% less) in the respective experiments. This is because the sorption data used in the core flooding simulations was obtained using powdered coal with 0.5 to 1 mm grain sizes. Zagorščak and Thomas [32] found that the CO_2 sorption capacity of an anthracite coal core (similar to core B) was 59% less than a powdered sample with 0.25 to 0.85 mm grain sizes, highlighting a limitation in applying sorption measurements on powdered coal to intact coal. This is controlled by the nature of coal porosity, which may be partitioned between open (passing, interconnected, dead-end) and closed pores [9]; powdering increases the sorption capacity by making open pores more accessible and by opening the closed pores. Since the ratios of the sorption capacities between N_2, CH_4 and CO_2 most likely remain similar for powdered and intact coal, it is not thought that the larger sorption capacities used had a significant impact on the results shown in Figure 7. Nonetheless, it highlights the importance

of using sorption data obtained using intact coal for numerical modelling, especially if the study is mainly concerned with identifying the amounts of gas stored or displaced.

In summary, the different stages of gas breakthrough for N_2 and CO_2 observed in the core flooding experiments were predicted in the numerical simulations. It is therefore concluded that the developed model is capable of simulating the main physical and chemical behaviour involved in gas flow in coal. Coal swelling was found to have a predominant effect on the multicomponent gas flow observed in the coal core flooding experiments. Although preferential displacement of CH_4 by CO_2 occurred, its effect on the observed gas breakthrough behaviour was limited by the short time scale of flow across the 120 mm long core relative to the CH_4 desorption kinetics. Hence, it is suggested that future work should further investigate the influence of core size on the observed behaviour.

6 Conclusions

A numerical investigation of coal core flooding with N_2 and CO_2 has been presented to validate the underlying theory of the model and provide further insights into behaviour observed in laboratory experiments. The model has been developed for studying the coupled flow and storage behaviour of dual porosity systems involving multiphase, multicomponent chemicals and gas. Hence, the work presented here serves to demonstrate the suitability of the model for simulating CO_2 sequestration in coal. This has been achieved by using data obtained in the laboratory testing of anthracite coal taken from the South Wales Coalfield, UK. This includes the key gas sorption and permeability data required as input to the model, and the use of multicomponent core flooding data as benchmarks for the main simulations.

The relationships used to describe adsorption-desorption kinetics and coal permeability changes during gas flow were found to provide a good fit with the experimental data. Moreover, the fitting process served to identify suitable values for the dual porosity material parameters, which are difficult to determine in the laboratory. These values were found to be similar to those reported in the literature for other coal. Two numerical simulations were performed, considering N_2 and CO_2 injection into a 120

mm long and 70 mm diameter coal core initially saturated with CH_4. Results were presented in terms of the effluent gas composition and it was found that the numerical model is able to predict the main stages of N_2 and CO_2 breakthrough. An analysis of physical and chemical behaviour showed that the breakthrough of N_2 was controlled by dual porosity gas flow without significant influence of adsorption-desorption. By comparison, adsorption-desorption and coal swelling were more important for CO_2 breakthrough. Coal swelling was identified as the predominant factor, with the effect of preferential displacement of adsorbed CH_4 by CO_2 being limited by the short time scale of flow across the 120 mm long core relative to the CH_4 desorption kinetics.

It was found that using sorption data obtained for powdered coal as input data for modelling an intact core will lead to the amount of gas storage being overestimated by a considerable amount. Since the ratios between the sorption capacities of N_2, CH_4 and CO_2 are the major factor influencing the nature of multicomponent gas breakthrough, this discrepancy with the experimental data was not apparent without the further analysis performed. However, it highlights that future numerical investigations should use sorption data obtained using intact coal. This will be especially important if the study is mainly concerned with identifying the amounts of gas stored or displaced.

In conclusion, the numerical model is capable of simulating the main physical and chemical behaviour involved in multicomponent gas flow and storage in coal. The insights provided in this work can be useful in the design of future experiments and it is recommended that studying the effects of core size on the observed behaviour would be particularly interesting. Furthermore, the use of detailed experimental data emphasised the importance of carefully selecting the input for numerical simulations. This is especially true for coal considering its highly complex and heterogeneous pore structure and the importance of coal-gas interactions.

Nomenclature

b_L^i Reciprocal of the Langmuir pressure (Pa^{-1})

c_β^i Concentration of the i^{th} gas component (mol m^{-3})

D_f^i Free fluid diffusion coefficient (m^2 s^{-1})

$D^i_{e,\beta}$	Effective diffusion coefficient (m^2 s^{-1})
k_β	Intrinsic permeability (m^2)
K	Bulk modulus (Pa)
n	Time step indicator (-)
n_β	Porosity (-)
n^L_F	Local fracture porosity (-)
$Q^i_{1,2}$	Adsorption capacity factors (-)
R	Universal gas constant (J mol^{-1} K^{-1})
R^i_s	Sink-source term due to sorption (mol m^{-3} s^{-1})
s^i_L	Langmuir adsorption capacity (mol kg^{-1})
s^i_r	Residual (unoccupied) adsorption capacity (mol kg^{-1})
s^i_s	Adsorbed amount (mol kg^{-1})
$s^i_{s,\infty,1,2}$	Adsorbed amounts at equilibrium (mol kg^{-1})
t	Time (s)
T	Temperature (K)
u_c	Hydrostatic confining pressure (Pa)
u_β	Gas pressure (Pa)
$\boldsymbol{v}_\beta$	Gas velocity (m s^{-1})
V^P_F	Volume of pores in the fracture zone (m^3)
V_F	Total volume of the fracture zone (m^3)
w_f	Volumetric weighting factor (-)
Z_β	Compressibility factor (-)
β	Coefficient linking the volumetric sorption strain to the matrix sorption strain
Γ^i_x	Sink-source term for inter-porosity mass exchange (mol m^{-3} s^{-1})
ε^S_b	Volumetric sorption strain (-)
ε^i_L	Langmuir strain (-)
μ_β	Absolute viscosity of the gas mixture (Pa s)
ρ_s	Coal density (kg m^{-3})
σ^i_D	First-order exchange rate due to diffusion (s^{-1})
τ_β	Tortuosity factor (-)
$\tau^i_{1,2}$	Adsorption rates (s^{-1})
ψ	Dimensionless factor relating to matrix block geometry (-)

Superscripts

i	Denotes the i^{th} gas component

Subscripts

F	Denotes the coal fracture network
M	Denotes the coal matrix pore region
β	Continuum identifier ($\beta = F$ or $\beta = M$)
χ_M^i	Mole fraction (-)

Acknowledgements

The financial support provided by the Welsh European Funding Office (WEFO), through the FLEXIS project, is gratefully acknowledged. The authors would like to thank Dr Majid Sedighi for his support.

References

1. Pan, Z., et al., *CO2 storage in coal to enhance coalbed methane recovery: a review of field experiments in China.* International Geology Review, 2017: p. 1-23.
2. van Bergen, F., H. Pagnier, and P. Krzystolik, *Field experiment of enhanced coalbed methane-CO2 in the upper Silesian basin of Poland.* Environmental Geosciences, 2006. **13**(3): p. 201-224.
3. Mazumder, S. and K.H. Wolf, *Differential swelling and permeability change of coal in response to CO2 injection for ECBM.* International Journal of Coal Geology, 2008. **74**(2): p. 123-138.
4. Connell, L.D., et al., *History matching of enhanced coal bed methane laboratory core flood tests.* International Journal of Coal Geology, 2011. **87**(2): p. 128-138.
5. De Silva, P.N.K. and P. Ranjith, *Advanced core flooding apparatus to estimate permeability and storage dynamics of CO2 in large coal specimens.* Fuel, 2013. **104**: p. 417-425.
6. Zhou, F.D., F. Hussain, and Y. Cinar, *Injecting pure N-2 and CO2 to coal for enhanced coalbed methane: Experimental observations and numerical simulation.* International Journal of Coal Geology, 2013. **116**: p. 53-62.
7. Wang, L., et al., *Comparison of enhanced coalbed methane recovery by pure N2 and CO2 injection: Experimental observations and numerical simulation.* Journal of Natural Gas Science and Engineering, 2015. **23**: p. 363-372.
8. Hadi Mosleh, M., et al., *Efficiency of carbon dioxide storage and enhanced methane recovery in a high rank coal.* Energy & fuels, 2017. **31**(12): p. 13892-13900.
9. Nie, B., et al., *Pore structure characterization of different rank coals using gas adsorption and scanning electron microscopy.* Fuel, 2015. **158**: p. 908-917.
10. Thomas, H.R. and Y. He, *Modelling the behaviour of unsaturated soil using an elasto-plastic constitutive relationship.* Géotechnique, 1998. **48**(5): p. 589-603.
11. Thomas, H.R., M. Sedighi, and P.J. Vardon, *Diffusive reactive transport of multicomponent chemicals under coupled thermal, hydraulic, chemical and mechanical conditions.* Geotechnical and Geological Engineering, 2012. **30**(4): p. 841-857.
12. Sedighi, M., H.R. Thomas, and P.J. Vardon, *Reactive Transport of Chemicals in Unsaturated Soils: Numerical Model Development and Verification.* Canadian Geotechnical Journal, 2016. **53**(1): p. 162-172.
13. Hosking, L.J., H.R. Thomas, and M. Sedighi, *A dual porosity model of high pressure gas flow for geoenergy applications.* Canadian Geotechnical Journal, 2018. **55**: p. 839-851.
14. Hadi Mosleh, M., et al., *High pressure gas flow, storage, and displacement in fractured rock—Experimental setup development and application.* Review of Scientific Instruments, 2017. **88**(1): p. 015108.

15. Hadi Mosleh, M., et al., *Carbon dioxide flow and interactions in a high rank coal: Permeability evolution and reversibility of reactive processes.* International Journal of Greenhouse Gas Control, 2018. **70**: p. 57-67.

16. Clarkson, C.R. and R.M. Bustin, *Coalbed methane: current evaluation methods, future technical challenges*, in *SPE Unconventional Gas Conference*. 2010: Pittsburgh, Pennsylvania.

17. Chung, T.H., et al., *Generalized Multiparameter Correlation for Nonpolar and Polar Fluid Transport-Properties.* Industrial & Engineering Chemistry Research, 1988. **27**(4): p. 671-679.

18. White, C.M., et al., *Sequestration of carbon dioxide in coal with enhanced coalbed methane recovery - A review.* Energy & Fuels, 2005. **19**(3): p. 659-724.

19. Chikatamarla, L., R. Bustin, and X. Cui, *CO2 sequestration into coalbeds: insights from laboratory experiments and numerical modeling*, in *Carbon dioxide sequestration in geological media - State of the science: AAPG studies in geology*. 2009, 457-474.

20. Palmer, I. and J. Mansoori, *How permeability depends on stress and pore pressure in coalbeds: a new model.* Spe Reservoir Evaluation & Engineering, 1988. **1**(6): p. 539-544.

21. Cui, X. and R.M. Bustin, *Volumetric strain associated with methane desorption and its impact on coalbed gas production from deep coal seams.* AAPG Bulletin, 2005. **89**(9): p. 1181-1202.

22. Robertson, E.P. and R.L. Christiansen, *A permeability model for coal and other fractured, sorptive-elastic media.* SPE Journal, 2008. **13**(3): p. 314-324.

23. Connell, L.D., M. Lu, and Z. Pan, *An analytical coal permeability model for tri-axial strain and stress conditions.* International Journal of Coal Geology, 2010. **84**(2): p. 103-114.

24. Harpalani, S. and G.L. Chen, *Estimation of Changes in Fracture Porosity of Coal with Gas Emission.* Fuel, 1995. **74**(10): p. 1491-1498.

25. Levine, J.R., *Model study of the influence of matrix shrinkage on absolute permeability of coal bed reservoirs.* In Gayer, R. & Harris, I. (eds.) Coalbed methane and coal geology, 1996: p. 197-212.

26. Seidle, J., *Fundamentals of coalbed methane reservoir engineering*. 2011, Tulsa, Oklahoma: PennWell Corporation.

27. Warren, J.E. and P.J. Root, *The Behavior of Naturally Fractured Reservoirs.* Society of Petroleum Engineers Journal, 1963. **3**(3): p. 245-255.

28. Hassanzadeh, H., M. Pooladi-Darvish, and S. Atabay, *Shape factor in the drawdown solution for well testing of dual-porosity systems.* Advances in Water Resources, 2009. **32**(11): p. 1652-1663.

29. Hadi Mosleh, M., *An experimental investigation of flow and reaction processes during gas storage and displacement in coal.* 2014, Cardiff University: Cardiff, UK.

30. Cui, X., R.M. Bustin, and G. Dipple, *Selective transport of CO2, CH4, and N2 in coals: insights from modeling of experimental gas adsorption data.* Fuel, 2004. **83**(3): p. 293-303.

31. Mastalerz, M., H. Gluskoter, and J. Rupp, *Carbon dioxide and methane sorption in high volatile bituminous coals from Indiana, USA.* International Journal of Coal Geology, 2004. **60**(1): p. 43-55.

32. Zagorščak, R. and H.R. Thomas, *Effects of subcritical and supercritical CO2 sorption on deformation and failure of high-rank coals.* International Journal of Coal Geology, 2018. **199**: p. 113-123.

33. Cussler, E.L., *Diffusion: mass transfer in fluid systems*. 2nd Edition ed. 1997, Cambridge: Cambridge University Press.